Int. J. Heat Mass Transfer. Vol. 30, No. 4, pp. 649–661, 1987
Printed in Great Britain

0017–9310/87 $3.00+0.00
Pergamon Journals Ltd.

Laminar flow past a sinusoidal cavity

C. SAIDI, F. LEGAY-DESESQUELLES and B. PRUNET-FOCH
Laboratoire d'Aérothermique du C.N.R.S., 4 ter, Route des Gardes, F-92190 Meudon, France

(*Received* 2 *April* 1986)

Abstract—The dynamic and thermal properties of a laminar flow past a sinusoidal cavity are studied. Velocity and temperature fields inside and above the cavity are numerically determined from the viscous flow equations. Results are compared with the experimental data obtained with a model placed in an incompressible and uniform flow. The good agreement with the dynamic field configuration allows the extension of these calculations to other sinusoidal wall geometries, to other main flow velocities and to cases with suction at the wall. Examples of streamlines and isotherms are given for these various situations.

1. INTRODUCTION

FLOWS and heat transfer in cavities of various shapes have been the subject of many publications in recent years [1–7]. Such studies are motivated by a desire to better understand the perturbations induced on the transfers at the wall by various surface irregularities.

The development of new low-velocity measurement techniques, such as laser anemometry, has made possible some of these studies [2]; simultaneously, the numerical resolution of the coupled Navier–Stokes and energy equations in the cavity [2–5] is now feasible with the high-speed and large memory computers.

This paper deals with the analytical and experimental study of heat transfer in laminar flow past a sinusoidal cavity of large amplitude/wavelength ratio. Various surface geometries and flow velocities are numerically investigated. Finally, the influence of suction at the wall is presented.

2. ANALYTICAL STUDY

Let us consider a sinusoidal cavity of amplitude a and wavelength λ (see Fig. 1). The fluid is assumed to be incompressible, Newtonian, with constant properties inside and over the boundary layer. Due to the low value of the Reynolds number, the flow is assumed to be steady and laminar. Effects of gravity and viscous dissipation are supposed to be negligible.

The dimensionless differential equations describing the velocity and temperature fields may be written in terms of stream function ψ, vorticity ω and temperature θ as

$$\omega = -\frac{\partial^2\psi}{\partial\bar{x}^2} + \frac{\partial^2\psi}{\partial\bar{y}^2} \tag{1}$$

$$Re\left(\bar{u}\frac{\partial\omega}{\partial\bar{x}} + \bar{v}\frac{\partial\omega}{\partial\bar{y}}\right) = \frac{\partial^2\omega}{\partial\bar{x}^2} + \frac{\partial^2\omega}{\partial\bar{y}^2} \tag{2}$$

$$Re\,Pr\left(\bar{u}\frac{\partial\theta}{\partial\bar{x}} + \bar{v}\frac{\partial\theta}{\partial\bar{y}}\right) = \frac{\partial^2\theta}{\partial\bar{x}^2} + \frac{\partial^2\theta}{\partial\bar{y}^2}. \tag{3}$$

Equation (3) has the same mathematical form as equation (2), but its boundary conditions are different.

2.1. *Boundary conditions*

Domain $\mathcal{D}$ is shown in Fig. 1. The boundary conditions relative to this physical situation are given below.

2.1.1. *At the wall.*

(1) For the stream function:

(a) when there is no slip at the wall and no injection nor suction through it

$$\left.\frac{\partial\psi}{\partial\bar{y}}\right|_w = \left.\frac{\partial\psi}{\partial\bar{x}}\right|_w = 0 \quad \text{and} \quad \psi_w = 0;$$

(b) when a uniform and vertical suction is imposed

$$\left.\frac{\partial\psi}{\partial\bar{y}}\right|_w = 0 \quad \text{and} \quad \left.\frac{\partial\psi}{\partial\bar{x}}\right|_w = -v_w$$

then ψ_w becomes a linear function of the abscissa x

$$\psi_w = -v_w x + \text{const.}$$

(2) The vorticity ω_w at the wall is deduced from equation (1) near the wall (cf. ref. [8]).

(3) The temperature is equal to T_w, which gives

$$\theta_w = 0.$$

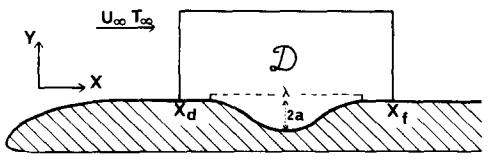

FIG. 1. Schematic configuration.

NOMENCLATURE

a	amplitude of the sinusoidal cavity [m]
D	reference length (taken here equal to the momentum thickness at x_d) [m]
dx, dy	mesh size in the x- and y-directions [m]
Pr	Prandtl number
Re	Reynolds number calculated with D
T	local temperature [K]
u, v	velocity components [m s^{-1}]
$\bar{u}, \bar{v}$	dimensionless components: $\bar{u} = u/u_\infty$; $\bar{v} = v/v_\infty$
x, y	coordinates defined in Fig. 1 [m]
$\bar{x}$	x/D
$\bar{y}$	y/D.

Greek symbols

$\alpha_1, \alpha_2, \alpha_3$	relaxation factors for the ψ, ω and θ difference equations, respectively
θ	dimensionless temperature, $(T - T_w)/(T_\infty - T_w)$
λ	wavelength
ν	kinematic viscosity
ψ	dimensionless stream function, (stream function/$u_\infty D$)
ω	dimensionless vorticity function, (vorticity/(u_∞/D)).

Subscripts

d	upstream abscissa of domain $\mathscr{D}$ (see Fig. 1)
f	downstream abscissa of domain $\mathscr{D}$
i, j	denotes position in the x- and y-directions
w	wall
∞	main flow.

Superscript

n	iteration index.

2.1.2. *In the main flow.*

$$\bar{u}_\infty = 1 \quad \text{which implies} \quad \frac{\partial \psi}{\partial \bar{y}} = 1$$

$$\omega = 0$$

$$T = T_\infty \quad \text{which implies} \quad \theta = 1.$$

2.1.3. *At the upstream boundary:* $x = x_d$. The profiles of the stream function $\psi(y)$ and the vorticity $\omega(y)$ are specified from Blasius' boundary layer theory on a flat plate at zero incidence with the previous boundary conditions in the main flow and at the wall.

The temperature profile $\theta(y)$ is directly deduced from the velocity $u(y)$ using the Crocco analogy which gives

$$\theta(\bar{y}) = u(\bar{y}).$$

It should be noted that the choice of such profiles is not very important, if the upstream boundary of domain $\mathscr{D}$ is far enough from the beginning of the cavity; computation shows that the results are not modified with another choice of the initial profiles.

2.1.4. *At the downstream boundary:* $x = x_f$. As previously, the imposed conditions are approximative by nature, since the cavity may indefinitely influence the external flow. The following relations were used:

$$\frac{\partial \psi}{\partial \bar{x}} = \text{const.}$$

$$\frac{\partial \omega}{\partial \bar{x}} = 0$$

and

$$\frac{\partial \theta}{\partial \bar{x}} = \text{const.}$$

These relations correspond to fully developed flow and temperature fields. However, several other conditions were tried and results were found to be similar.

2.2. *Numerical treatment*

With the boundary conditions, the system of differential equations cannot be solved analytically and so numerical techniques must be employed. The use of a finite difference method enables us to transform the three partial differential equations into algebraic ones. The choice of the general mesh system for domain $\mathscr{D}$ has a predominant influence on the convergence of the calculations.

A non-uniform, rectangular grid was chosen with a varying mesh spacing throughout the domain. The grid in Fig. 3 is shown for illustration purposes only; it does not represent exactly the meshes which were used.

In the cavity, the mesh size was kept constant along the x-axis, whereas along the y-axis it was determined in order to have nodes lying just upon the sinusoidal wall. Hence, the wall vorticity ω_w is easily evaluated without any interpolation.

Outside the cavity, the mesh size along the x-axis was kept constant. Along the y-axis: between 0 and $y = D$ (where D is the boundary layer thickness at the abscissa x_d) the mesh was also kept constant; for $y > D$, mesh sizes were determined in arithmetical

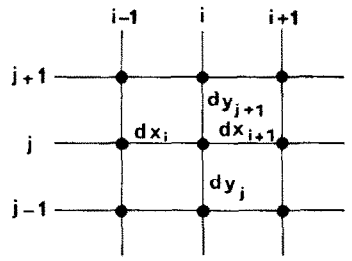

FIG. 2. Sketch of general grid.

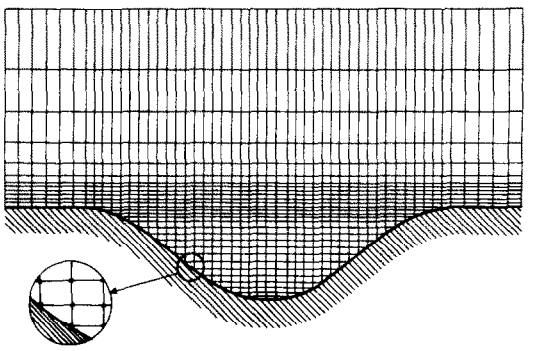

FIG. 3. System of nodal points.

progression. In this way the position of the upper boundary of domain $\mathscr{D}$ can be modified without increasing the number of meshes, only the factor of the progression is changed. With this possibility, the distance over which the solution is not influenced by this position can be estimated; in the present applications a distance of $7D$ was found to be sufficient.

2.3. *Discretization*

Equations (1)–(3) are discretized as follows:

(1) For the diffusion terms, 'central differences' are used

$$\frac{\partial^2\phi}{\partial\bar{x}^2} = 2\frac{\mathrm{d}\bar{x}_i\phi_{i+1,j} - (\mathrm{d}\bar{x}_i + \mathrm{d}\bar{x}_{i+1})\phi_{ij} + \mathrm{d}\bar{x}_{i+1}\phi_{i-1,j}}{\mathrm{d}\bar{x}_i\mathrm{d}\bar{x}_{i+1}(\mathrm{d}\bar{x}_i + \mathrm{d}\bar{x}_{i+1})}$$

where $\phi_{i,j}$ is the value of any function ϕ at the i,jth node of the grid; this is illustrated in Fig. 2. ϕ is used for the function ψ, ω or θ.

(2) For the convection terms, 'upwind differences' are used (cf. ref. [11]). They may be expressed as

$$\bar{u}\frac{\partial\phi}{\partial\bar{x}} = \bar{u}\frac{\phi_{i,j} - \phi_{i-1,j}}{\mathrm{d}\bar{x}_i} \quad \text{if } \bar{u} > 0$$

$$\bar{u}\frac{\partial\phi}{\partial\bar{x}} = \bar{u}\frac{\phi_{i+1,j} - \phi_{i,j}}{\mathrm{d}\bar{x}_{i+1}} \quad \text{if } \bar{u} < 0$$

with equivalent formulae along the y-axis.

When the differential terms are replaced by these algebraic quantities in the three equations, an iterative calculation is used. At each iteration, the new solutions of the three equations are derived from the previous calculated fields. These calculations are repeated until the difference between two successive iterations is smaller than 5/10,000 for the three functions. To start this iterative procedure a judicious arbitrary repartition of ψ, ω and θ in the whole domain is used; it was found that Blasius' initial profiles over the cavity and values equal to zero inside the cavity provided good initial profiles.

This convergence procedure is largely improved by using the relaxation method, where the values ψ^c, ω^c and θ^c directly computed from the equations are corrected by $\psi^{(n-1)}$, $\omega^{(n-1)}$ and $\theta^{(n-1)}$, given at the $(n-1)$th iteration, as

$$\psi_{i,j}^{(n)} = (1-\alpha_1)\psi_{i,j}^{(n-1)} + \alpha_1\psi_{i,j}^c$$

$$\omega_{i,j}^{(n)} = (1-\alpha_2)\omega_{i,j}^{(n-1)} + \alpha_2\omega_{i,j}^c$$

$$\theta_{ij}^{(n)} = (1-\alpha_3)\theta_{i,j}^{(n-1)} + \alpha_3\theta_{i,j}^c$$

where α_1, α_2, α_3 are relaxation coefficients.

The stability of the solution depends essentially upon the choice of the relaxation parameters, the mesh size and the treatment of the convection terms.

For the stream function ψ, a constant relaxation coefficient α_1 can be taken. However, relaxation of the vorticity with a constant coefficient α_2 leads to dramatic instabilities as observed by Johnson and Dhanak [5]. They suggested that, for a rectangular cavity, the coefficient α is a function of the local velocity at each step. In the present work, this coefficient α_2 is in a similar form, but the mesh sizes in the x- and y-directions being neither equal nor regular, the absolute value of the difference in velocities at each node was taken into account, in the following way:

$$\alpha_2 = \frac{k_1}{k_2 + Re\dfrac{\mathrm{d}y_j\,\mathrm{d}y_{j+1}}{\mathrm{d}x_i}|\bar{u} - \bar{v}|}$$

where k_1 and k_2 are constants; for experimental conditions, they are equal to 3 and 4, respectively; so, α_2 is varying between 0.1 and 0.75 whereas α_1 is equal to 1.2.

For the temperature field, the energy equation is analogous to the momentum one, thus α_3 has the same expression as α_2, with $Re\,Pr$ instead of Re.

When these coefficients are judiciously chosen, convergence was always obtained in less than 800 iterations. If more iterations are performed the convergence improves regularly; typical solution times required 1–2 min for 800 iterations on the NAS-AS/9080.

3. EXPERIMENTAL PROCEDURE AND RESULTS

3.1. *Experimental devices*

Experiments were carried out at atmospheric pressure, in a low-speed wind tunnel, the characteristics of which are presented in refs. [9, 10]. The temperature

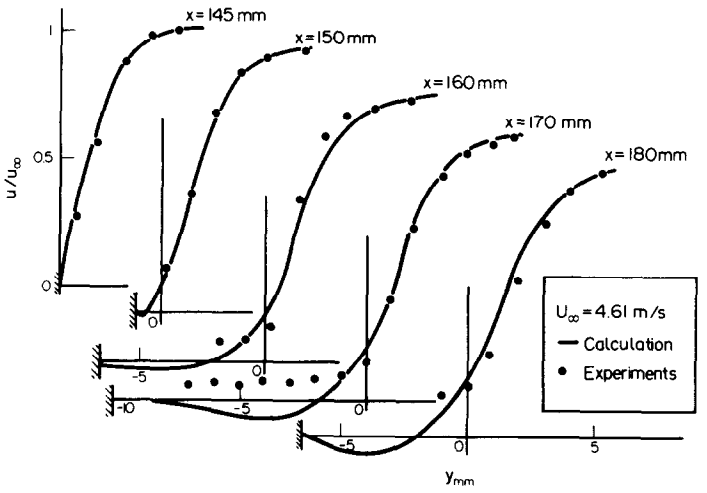

FIG. 4. Experimental and calculated velocity profiles.

of the fluid is controlled with an electrical air heater. The test plate, made of brass, has an elliptic leading edge, then is flat and further downstream, wavy. The amplitude of the waves is equal to 5 mm, the wavelength is 50 mm. The test plate is heated by a circulation of warm water; its uniform temperature is lower than that of the main flow.

Velocity measurements are performed by laser anemometry and local temperatures are measured by means of a thermocouple probe which can be placed at various locations in the boundary layer. Experimental velocity and temperature profiles are plotted by a data acquisition system.

3.2. *Results and discussion*

By fitting the numerical calculation data with the experimental conditions, a comparison can be made between calculations and experiments. The main flow velocity was 4.6 m s^{-1} and the temperature 85°C; the beginning of the cavity is located at an abscissa equal to 0.15 m. A range of velocity profiles are shown in Fig. 4 at several abscissae on the sinusoidal surface. Over the flat part of the plate, experimental and calculated profiles are identical and very close to that of Blasius. At other abscissae, the agreement is rather good outside the cavity; however, inside it, experiments were performed without a Bragg cell so that only the absolute horizontal component of the velocity is obtained, this is why the agreement is not very good.

In Fig. 5, the calculated velocity profiles are plotted along the sinusoidal surface; it may be observed that separation occurs near the beginning of the cavity ($x = 0.16$ m), and that the negative velocities remain quite small. The reattachment point is around $x = 0.19$ m. At $x = 0.2$ m, i.e. on the flat part after the cavity, the velocity profile is close to that of Blasius. It can be said that relaminarization occurs; however, fluctuations induced by the vortex inside the cavity are obviously present; perhaps, the transition region is already triggered by these fluctuations. By comparison with a flat plate, the local skin friction coefficient is reduced by the wavy wall; however, the transition point is advanced [8].

In Fig. 6, several temperature profiles are exhibited at various abscissae. The main flow velocity was again 4.6 m s^{-1}, its temperature was 85°C, and the temperature difference between the main flow and the wall was 15°C. As for the velocity, calculated temperature profiles are in good agreement with measured points above the flat part and the cavity. Inside the cavity, an important discrepancy between calculation and measurements should be noted. This difference is not due to the free convection terms which were neglected; when they are taken into account in equation (2), results are unchanged.

This viscous dissipation cannot either explain this difference as long as the velocity gradients are low (Fig. 4). Such a discrepancy may be due to the tridimensional and unsteady effects induced by the vortex, since the local temperature is increased by hot air circulation.

Nevertheless, for the dynamic point of view, the agreement between calculation and experiments is good enough to allow application of this calculation procedure to other wall geometries and different Reynolds numbers.

3.3. *Influence of the wall geometry*

For the same Reynolds number as used previously and for the same wavelength, the amplitude of the sinusoidal wall has been put successively equal to 10^{-2} and 2.5×10^{-2} m and results have been compared to the previous case where $a = 5 \times 10^{-3}$ m. Note that this amplitude cannot be much smaller than 5×10^{-3} m, since the mesh spacings become too small and convergence cannot be reached.

In Fig. 7, streamline patterns within and above the cavity are drawn from the calculated stream function values by interpolating between points when neces-

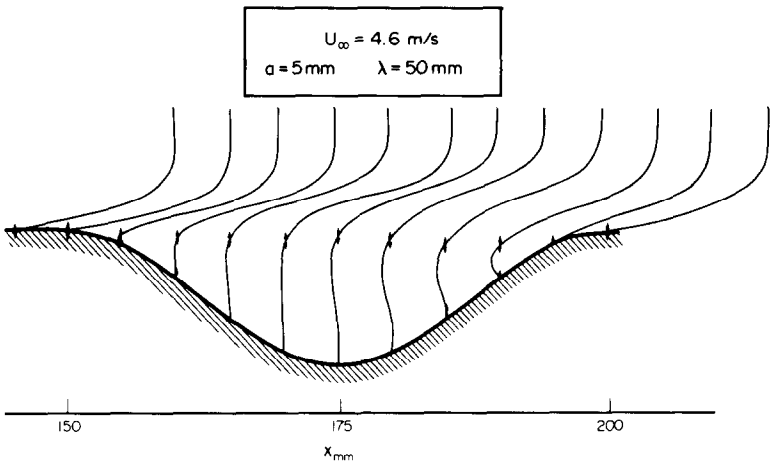

FIG. 5. Evolution of velocity profiles along the wavy wall.

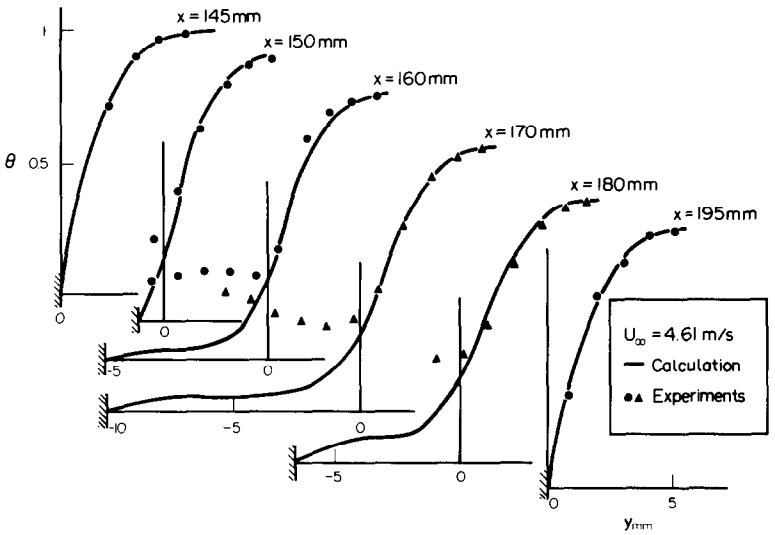

FIG. 6. Experimental and calculated dimensionless temperature profiles.

sary, for the three values of the amplitude. It may be observed that the secondary vortex, present when $a = 5 \times 10^{-3}$ m, becomes greater and greater when the amplitude increases while the principal vortex becomes flatter near the top of the cavity. Moreover, the separation point goes upstream and the reattachment point downstream.

Isotherms which are also obtained by a linear interpolation are shown in Fig. 8 for these three amplitudes. From this figure, it can be shown that the total heat exchange at the wall is reduced by the presence of the cavity since the vortex plays the role of a thermal screen which creates a large region of uniform temperature in the bottom of the cavity.

3.4. *Influence of the flow velocity*

With the first wall geometry ($a = 5 \times 10^{-3}$ m and $\lambda = 5 \times 10^{-2}$ m), calculations were performed for various flow velocities. As an example, streamline patterns are shown in Fig. 9 for three values of $u_\infty = 0.5$, 7 and 15 m s^{-1} which correspond to Reynolds numbers (based on momentum thickness) of about 40, 140 and 200, respectively. The vortices which are present in this figure, increase in size and in number as the flow velocity increases. Only one vortex appears for the lowest velocity, a secondary vortex is present and large enough for $u_\infty = 7$ m s^{-1} and a small third one develops at the bottom of the cavity for $u_\infty = 15$ m s^{-1}. The main flow is more and more insensitive to the presence of the cavity as flow velocity increases.

For the same three cases, isotherms are drawn in Fig. 10; as previously, it can be seen that temperature gradients are regular enough for the low flow velocity, $u_\infty = 0.5$ m s^{-1}, isotherms warp when $u_\infty = 7$ m s^{-1} and become really asymmetric for $u_\infty = 15$ m s^{-1}. This may be due to the presence of the third vortex.

3.5. *Wall suction*

The comparison of a condensation phenomena with wall suction revealed some similarities as shown

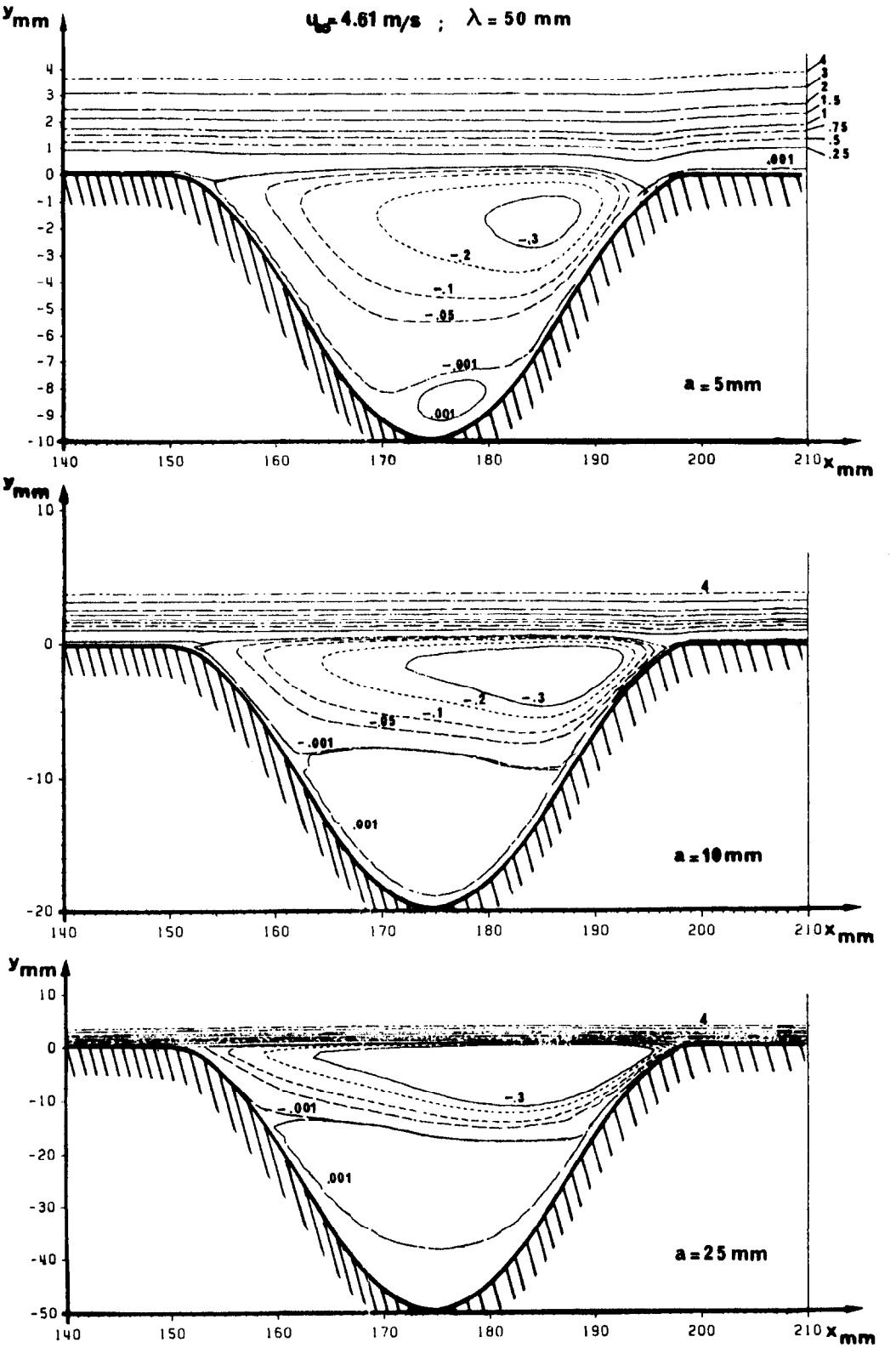

FIG. 7. Analytical streamline patterns for different values of amplitude a.

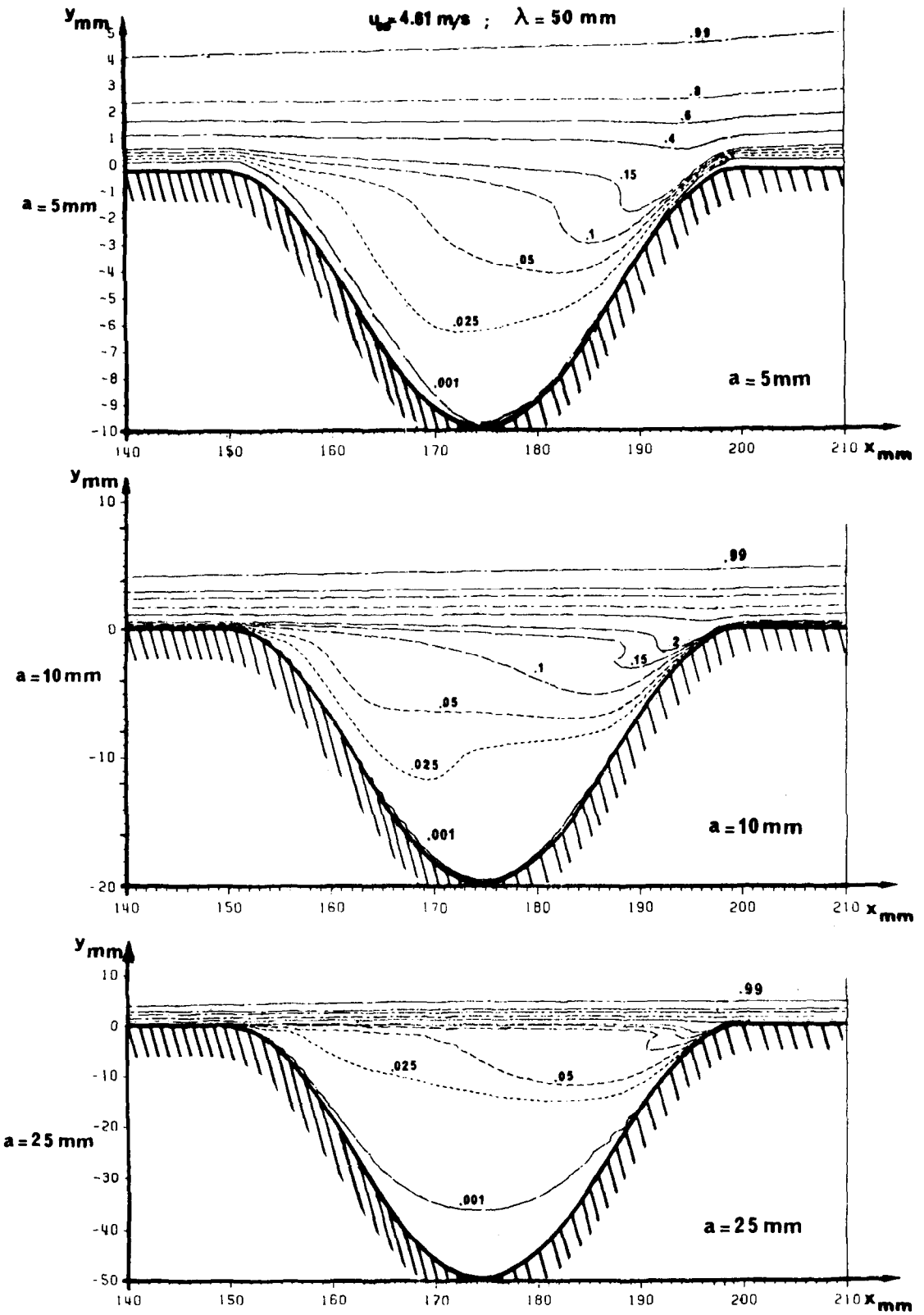

FIG. 8. Analytical isotherm patterns for different values of amplitude a.

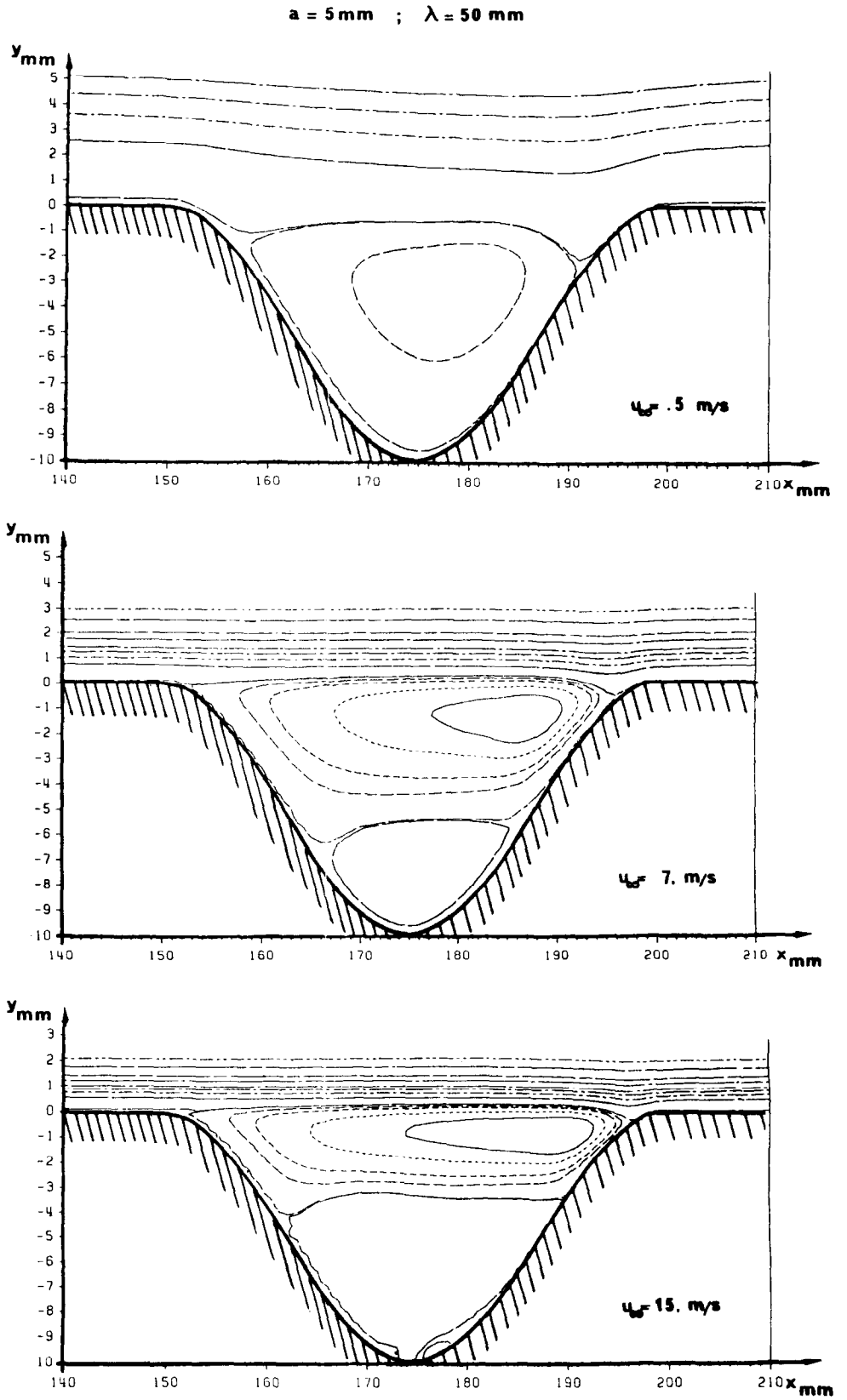

FIG. 9. Influence of main velocity on streamline patterns.

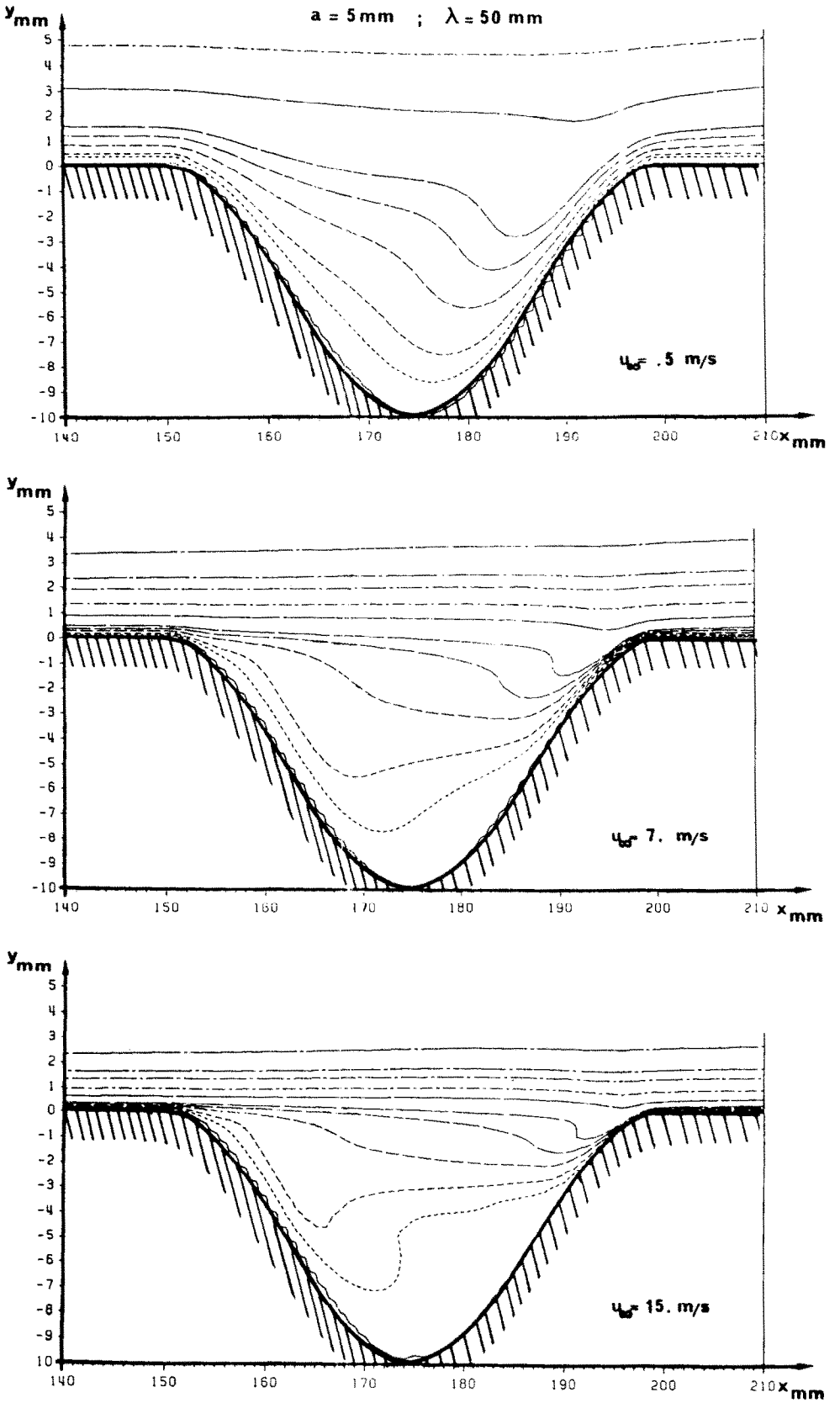

FIG. 10. Influence of main velocity on isotherm patterns.

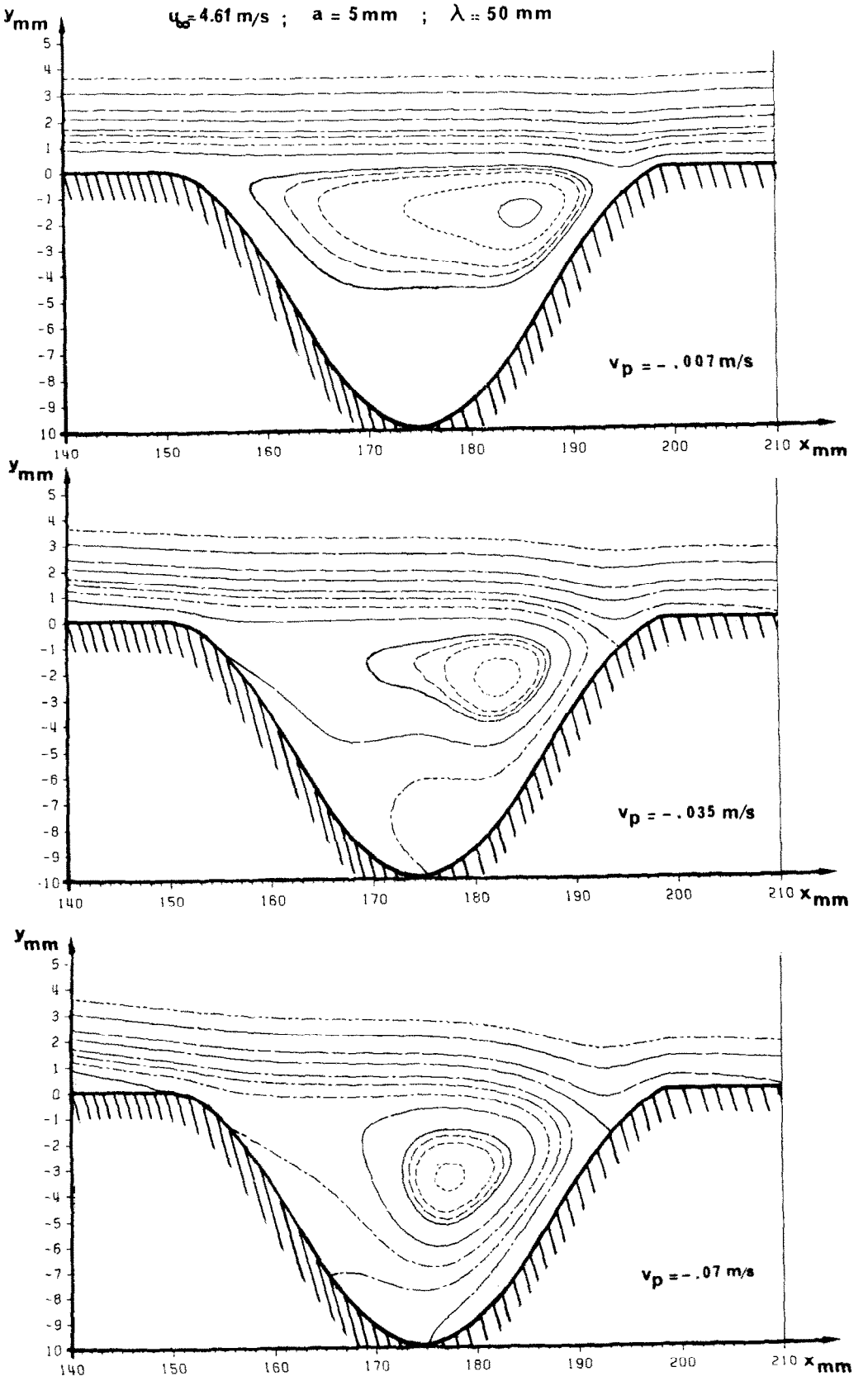

FIG. 11. Effect of vertical suction on streamline patterns.

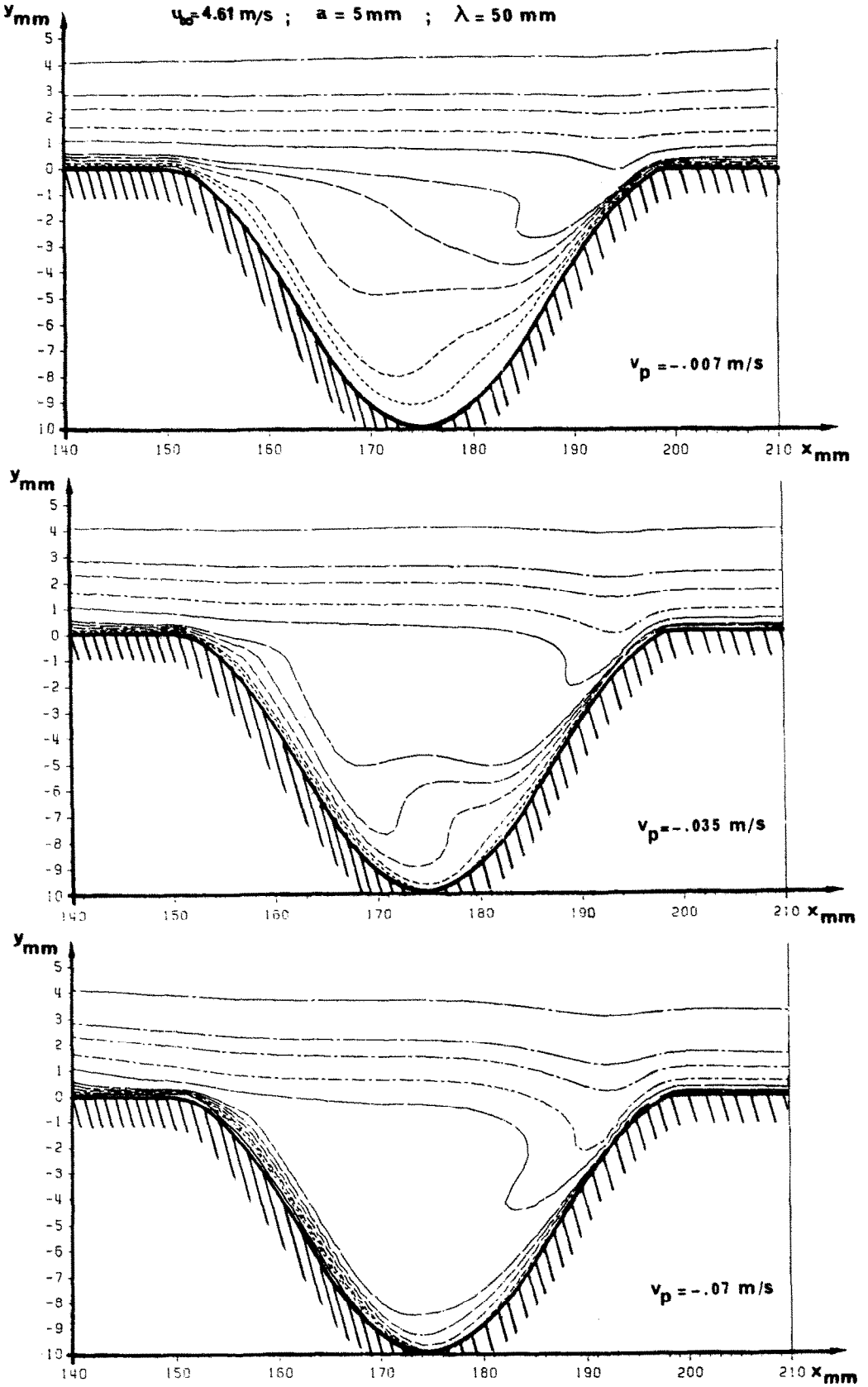

FIG. 12. Effect of vertical suction on isotherm patterns.

in ref. [10]. It may be of interest to know how, for this kind of sinusoidal cavity, the flow field is influenced by suction.

If a suction of constant rate is applied along the wall boundary in the y-direction as in ref. [10], velocity and temperature fields are modified.

The analytical study of the problem remains the same; only the boundary condition for ψ at the wall is different, as stated before. It should be noted here that, with such a suction in the y-direction: $u_w = 0$, $v_w = v_p < 0$; so, along the sinusoidal boundary, the tangential velocity is not zero, and there is slip at the wall. In Figs. 11 and 12, streamline patterns and isotherms are respectively exhibited for three different suction rates. The separation point is suppressed by suction whereas a vortex is always present. It can be observed that isotherms enter deeper and deeper into the cavity so that temperature gradients increase with the rate of suction.

4. CONCLUSION

A solution of the dynamic and thermal problem of a fluid flowing above a sinusoidal cavity with or without suction was presented in this paper, when the boundary layer is supposed to be laminar. The flow equations were solved by using finite differences with a relaxation method. Rapid convergence towards stable solutions was obtained with well-chosen relaxation coefficients.

(1) From the dynamic point of view, experiments were in good agreement with theoretical results. For instance, the vortex inside the cavity is well predicted.

(2) For the thermal field, outside the cavity the agreement between computed results and experiments is also good. However, inside the cavity, some discrepancies appear, which may be due to the assumption of a bidimensional flow; the vortex can induce tridimensional effects which were not taken into account. Hence, heat exchange at the wall is minimized in the computation.

Extensions of the calculation to other cases show that even for slow velocities, the vortex fills up the cavity, so the outer flow is only slightly modified by the wall deformation. Moreover, for a given cavity, when the velocity is greater, the first vortex gives birth to two or more vortices. If, for a fixed main flow velocity and for a constant wavelength, the amplitude of the deformation is increased, the secondary vortex occupies more than half the volume of the cavity. Finally, the effect of suction at the wall can be predicted.

REFERENCES

1. R. D. Mills, Numerical solution of viscous flow equations for a class of closed flows, *J. R. aeronaut. Soc.* **69,** 714–718 (1965).
2. D. Bellet, D. P. Ly and M. Milleret, Steady laminar flows between a ball and a spherical cavity, *Trans. Am. Soc. mech. Engrs*, Series E, *J. appl. Mech.* **51,** 6–12 (1984).
3. H. Inaba and N. Seki, Natural convective heat transfer in a shallow rectangular cavity with different end temperatures, *Numer. Heat Transfer* **4,** 1459–1468 (1981).
4. A. Bhatti and W. Aung, Finite difference analysis of laminar separated forced convections in cavities, *Trans. Am. Soc. mech. Engrs*, Series C, *J. Heat Transfer* **106,** 49–54 (1984).
5. R. W. Johnson and A. M. Dhanak, Heat transfer in laminar flow past a rectangular cavity with fluid injection, *Trans. Am. Soc. mech. Engrs*, Section C, *J. Heat Transfer*, **98,** 226–231 (1976).
6. A. K. Gupta and E. L. Mollo-Christensen, An experimental investigation of air flow over a wavy plate, Massachussets Institute of Technology, Aeroelastic and Structures Research Laboratory (1966).
7. B. Prunet-Foch, Etude des décollements, en écoulement isovolume se produisant sur une plaque plane à paroi sinusoïdale, Thèse de 3ème Cycle, Université de Paris (1969).
8. C. Saidi, Transferts de chaleur et de masse dans une cavité sinusoïdale placée dans un écoulement laminaire incompressible constitué d'air pur ou d'un mélange saturé en vapeur, Thèse de 3ème Cycle, Université Paris VII (1985).
9. F. Legay-Désesquelles, Etude théorique et expérimentale du transfert de chaleur et de masse dans une couche limite incompressible avec condensation sur une plaque plane, Thèse d'Etat, Université Paris VI (1984).
10. F. Legay-Désesquelles and B. Prunet-Foch, Dynamic behaviour of a boundary layer with condensation along a flat plate: comparison with suction, *Int. J. Heat Mass Transfer* **28,** 2363–2370 (1985).
11. F. M. White, *Viscous Fluid-flow*, pp. 217–224. McGraw-Hill, New York (1974).

ECOULEMENT LAMINAIRE AU-DESSUS D'UNE CAVITE SINUSOÏDALE

Résumé—L'étude porte sur le comportement dynamique et thermique d'un écoulement d'air au-dessus d'une cavité sinusoïdale. Une résolution numérique des équations de Navier–Stokes et de l'énergie a permis de déterminer les champs de vitesse et de température à l'intérieur de la cavité et au-dessus. Les résultats ont été confrontés aux mesures réalisées à l'aide d'une maquette placée dans un écoulement uniforme incompressible. Le bon accord obtenu sur la définition du champ dynamique de l'écoulement a conduit à appliquer le calcul à diverses géométries de paroi, à différentes vitesses de l'écoulement et à des cas où existe une aspiration à la paroi. Pour chaque résultat, les lignes de courant et les isothermes sont fournis.

LAMINARE STRÖMUNG ENTLANG DEN SINUSFÖRMIGEN WÄNDEN EINES HOHLRAUMS

Zusammenfassung—Die dynamischen und thermischen Eigenschaften einer laminaren Strömung entlang den sinusförmigen Wänden eines Hohlraums werden untersucht. Die Geschwindigkeits- und Temperaturverteilungen innerhalb und oberhalb des Hohlraums werden aus den Strömungsgleichungen numerisch berechnet. Die Rechenergebnisse werden mit solchen experimentellen verglichen, welche in einer gleichförmigen, inkompressiblen Strömung ermittelt worden waren. Die gute Übereinstimmung mit dem dynamischen Feldverlauf gestattet die Übertragung der Berechnungen auf andere sinusförmige Wandungen, andere Hauptströmungs-Geschwindigkeiten und auf Fälle mit Absaugung an der Wand. Es werden Beispiele der Stromlinien und der Isothermen für diese unterschiedlichen Bedingungen angegeben.

ЛАМИНАРНОЕ ТЕЧЕНИЕ ЗА СИНУСОИДАЛЬНОЙ ПОЛОСТЬЮ

Аннотация—Исследованы динамические и тепловые характеристики ламинарного течения за синусоидальной полостью. Поля скорости и температуры внутри и над полостью найдены численно из уравнений вязкого течения. Результаты сравниваются с экспериментальными данными для модели, помещенной в однородный поток несжимаемой жидкости. Хорошее соответствие с конфигурацией динамического поля дает возможность применять данные результаты для других геометрий синусоидальной стенки, для других скоростей основного потока и для случаев отсоса на стенке. Представлены примеры линий тока и изотерм для различных случаев.